Microbubble Enhanced Bitumen Separation from Tailing Slurries with High Solid Contents

Kaiyu Zhou,[†] Somasekhara Goud Sontti,[†] Joe Zhou,[‡] Payman Esmaeili,[¶] and Xuehua Zhang[*,†]

[†]*Department of Chemical and Materials Engineering, University of Alberta, Alberta T6G 1H9, Canada*

[‡]*Disruptive Separation Technology Ltd.(DSTL), Edmonton, Alberta T6X 1M5, Canada*

[¶]*Imperial Oil, Calgary, Alberta T2C 4P3, Canada*

E-mail: xuehua.zhang@ualberta.ca

Abstract

Removing bitumen from oil-sands tailings reduces greenhouse gas emission during waste disposal. However, it is technically challenging to efficiently recover bitumen residual in tailing slurries with high solid contents, due to the tiny fraction of bitumen and complicated composition in the tailings. This work focuses on microbubble-enhanced bitumen recovery in a flow of artificial tailings that consisted of 50 wt% solids, 0.2 wt% bitumen and 49.8 wt% process water. Using a laboratory–scale transport pipeline loop, we show that several operation conditions had a positive impact on the efficiency of bitumen recovery, including bubble formation from intensified cavitation, the addition of gas integrated with cavitation, or increasing the temperature up to 52 °C. The efficiency of bitumen recovery was even higher from the addition of CO_2 bubbles compared to air bubbles. Under optimal conditions, more than 61 % bitumen was recovered from an extremely initial fraction of 0.2 wt% with the generation of microbubbles. This work provides guideline in finding an effective combination

of operational conditions for bitumen separation from hydrotransported real tailings containing high solid content. The same approach may be also applicable for cleaning of oil contaminated slurries.

1 Introduction

In pursuit of sustainable development, much effort has been paid to separation of toxic or hazardous materials of particular concern in bulk industrial wastewater. Oil sand tailings contain clays, sands, residual bitumen and organic chemicals.[1,2] Bitumen residues in the tailing ponds form harmful components released to environment with time and create hazardous habitation for the wildlife. In addition to the urgency of reducing environmental footprint and greenhouse gas (GHG) emissions, recovering residual bitumen contents from the tailings using CO_2 bubbles can favorably speed up the process of consolidation and water release characteristics and shorten the time required for land reclamation.[3,4]

As one of the most widely used techniques for particle separation, bubble flotation has benefited significantly from nanoscale phenomena by using micro and nanobubbles for enhancing sustainability.[5,6] Technical advantages exhibited in microbubble floating extraction are high separation efficiency and low economic costs.[6] Several works demonstrated applications of microbubble floating extraction for recovering valuable metals from dilute aqueous solutions.,[7,8] for instance, the separation of low concentrations of molybdenum from tungstate solutions.[9] In contrast, bitumen recovery technology is scarce from oil sand tailings for distinct solid distributions under industrial operational conditions. Moreover, a standard process in flotation separation may require the construction of new facilities and extra time to process the massive volume of tailings produced on the industrial scale. An innovative strategy is to recover bitumen residue during the hydrodynamic transport of coarse tailings to the tailing ponds.[10] Bitumen recovery from the tailing flow is desirable as the separation process may leverage the pipeline systems in current operation. For highly efficient recovery during pipeline hydrotransport, it is essential to enhance bitumen separation in the

slurry flow.

Flow behavior of concentrated tailings slurry in the pipeline can be highly complex, influenced by flow velocity,[11] solid concentration, physical properties of carrier liquids, and solid size distribution.[12,13] Non–Newtonian carrier flow consists of water and fine particles (<45 μm). The flow regimes strongly depend on the flow rate. A broad classification of flow regimes is pseudo–homogenous or heterogeneous flow, or a layered flow such as two or threeflow, corresponding to slurry/suspension flow rate.[14,15] A considerably high flow rate develops a pseudo–homogeneous flow pattern where uniform particle distribution is observed across the liquid phase at any position through the flow direction. Similarly, intermediate flow rates form a heterogeneous flow regime where a non–uniform particle distribution develops across the liquids phase. Most particles move along the lower part of the pipe. For lower flow rates, continuous bed forms at the bottoms of the pipe move along the lower pipe wall, where a heterogeneous flow pattern forms in the upper layer of the moving bed.[16,17] Further decreasing the flow rate to a lower range, the solid particles accumulate at the bottom of the pipe resulting in stationary particles deposition with a densely packed layer.[18]

Recent research shows that injection of microbubbles to a slurry flow in a labscale pipeline could significantly increase the efficiency of bitumen separation from diluted sand dispersion from 10% to more than 50%.[10] However, it remains unclear how microbubbles in the flow may impact separation of residual bitumen in highly concentrated tailing slurries. The interactions between bitumen, or solid particles and bubbles in the slurry have been investigated extensively in standard flotation processes. In a separation column, air bubbles attach to bitumen droplets to form bitumen–bubble aggregates with low density for efficient flotation.[19–21] Notably, the bubble size plays a major role in interactions between bitumen droplets and bubbles.[21] For the probability of a bitumen droplet captured by a bubble, P_{Cap}, is defined as follows:[21,22]

$$P_{Cap} = P_c \times P_a \times P_s \tag{1}$$

Where P_c, P_a and P_s are the probability of bitumen–bubble collision, bitumen–bubble attachment and bitumen–bubble stability, which depend on the bubble size. Tiny bubbles tend to have a high surface–to –volume ratio, thereby improving the possibility of collision between bitumen droplets and bubbles. The long residence time of tiny bubbles supplies sufficient time for attachment.[23–25] Nanobubbles in a solid surface can enhance the attachment of a larger floating bubble to the substrate.[23] Tiny bubbles coalesce with flotation bubbles, thus accelerating the film drainage between flotation bubbles and bitumen droplets.[26] Inversely, large–flotation bubbles cannot capture tiny bitumen droplets directly.[27] Clusters formed by microbubbles and bitumen droplets tend to attach to such large bubbles via coalescence of bubbles. Therefore, a more significant rise velocity of the clusters is gained due to the higher buoyancy force. The synergic effect of small and large bubbles improves bitumen recovery generally.[21]

Generation of microbubbles has experienced rapid development of many technologies, such as acoustic cavitation,[28,29] hydrodynamic cavitation[30] and optic cavitation.[31] Among different categories of cavitation, hydrodynamic cavitation by a venturi–type the generator has the advantage of low energy intensity, high efficiency, and simple structure, and is considered a promising method for microbubble generation in industrial processes.[32] For a conventional venturi tube composed of a converging section, a throat and a diverging section, bubble formation is based on the principle of Bernoulli effect.[33] In the throat, an increase in the flow velocity and a drop in the pressure occur simultaneously. The local pressure dropping below the vapor pressure contributes to formation of a large number of vapor bubbles. Furthermore, gas suction can be employed by adding an opening at the throat at low pressure.[33,34] The turbulent hydrodynamic flow breaks up those air slugs into small bubbles.

Apart from the air as the gas source, CO_2 has attracted significant attention in the oil sands industry. It is well known that CO_2 has a higher solubility compared with air.[35] The dissolved CO_2 decreases the pH of the liquid for faster sedimentation of mature fine tailings in the ponds.[36] The vapor bubbles generated by cavitation are stabilized by dissolved gas

as well. Moreover, the bitumen-bubble aggregates can be formed by gas nucleation. The dissolved CO_2 nucleates on the hydrophobic surfaces and grows when the temperature and pressure change.[36] Such a process excludes the bitumen–bubble collision and attachment.

Temperature is crucial for recovering bitumen in the oil sand industry.[13,37,38] On the one hand, the temperature dramatically impacts cavitation behavior. Increasing the temperature raises the vapor pressure of water and throat pressure which are incompatible with cavitation.[39] The higher temperature leads to rapid bubble formation but destabilizes the microbubbles generated by cavitation.[27,33] On the other hand, the increase in the temperature decreases the viscosity and density of bitumen. With the addition of microbubbles, the low bitumen viscosity strengthens the stability of bitumen–bubble aggregates by engulfment.[13,40] The decreased bitumen density benefits the separation of bitumen a lot. In addition, the effect of temperature on solid–bubble interaction has been investigated in the literature. It is found that slime coating has prohibited bubbles from contacting with bitumen droplets and hence reduced separation efficiency and froth quality.[13] Increasing the temperature decreases adhesion between fines and bitumen and enhances repulsive force between other solid particles and bitumen within a small distance.[41] The weakened coverage of bitumen by mineral particles enhances the interaction with bubbles.

In this study, experimental study was conducted to idenfity the effects of microbubbles on the bitumen recovery from the flow of a high solid concentration tailing slurry. The solid content in our highly concentrated slurry of artificial tailings was as high as 50 wt%. A laboratory–scale transport pipeline loop was employed to process the tailing slurry at various flow velocities, temperatures, and gas types. A 3D–printed venturi tube was used to generate microbubbles from cavitation combined with suction of air and CO_2 at the upstream of the trough of the pipeline loop. The effect of each variable was identified based on the difference in the bitumen recovery. In order to have a better understanding of effects of microbubbles in recovering residual bitumen, the focused beam reflectance measurement (FBRM) technique was applied to record the number of microbubbles in the process water. It was found that

the temperature and the solubility of gas significantly influence the number of microbubbles. This work will help determine the optimal operating conditions for bitumen recovery from the flow of tailings in a pipeline.

2 Experimental Section

2.1 Laboratory Hydrotransport Pipeline Loop

The laboratory hydrotransport pipeline loop is a versatile setup utilized to control various combinations of operating parameters in the processing of oil sand tailings. The injection of bubbles can occur at different locations along the pipeline to recover bitumen, depending on the bubble generation method. Figure 1(a) provides a schematic of the pipeline loop system, which includes collection trough, progressive cavity pump, double pipe heat exchanger, drain valve and ball valve.[37]

The loop pipeline was stainless steel with 200 cm in length, 68 cm in height and an inner diameter of 2.2 cm. A transparent section was made of resistant glass with 40 cm in length and an inner diameter of 17 mm. It allows the visualization of the tailing slurry. At the right of the glass section, a trough serves both as the inlet feed location and a collection point for floated froth. A low-speed progressive cavity pump installed vertically at the right part of the loop was used to circulate fluid in the pipeline loop. The rotational speed of the cavity pump was controlled by a 3 HP variable AC power supply. A double pipe heat exchanger connected to a programmable circulating bath was utilized to control the fluid temperature in the pipeline loop. The outflow of the heat exchanger could be cooled down or heated up to the set temperature with LabVIEW, which was used to control the programmable water bath. Moreover, a mercury thermometer was employed at the trough location to validate the temperature readings of the thermometer probe within the loop. The ball valve at the top was used as the microbubble injection location and a sampling point for fluids. The lower

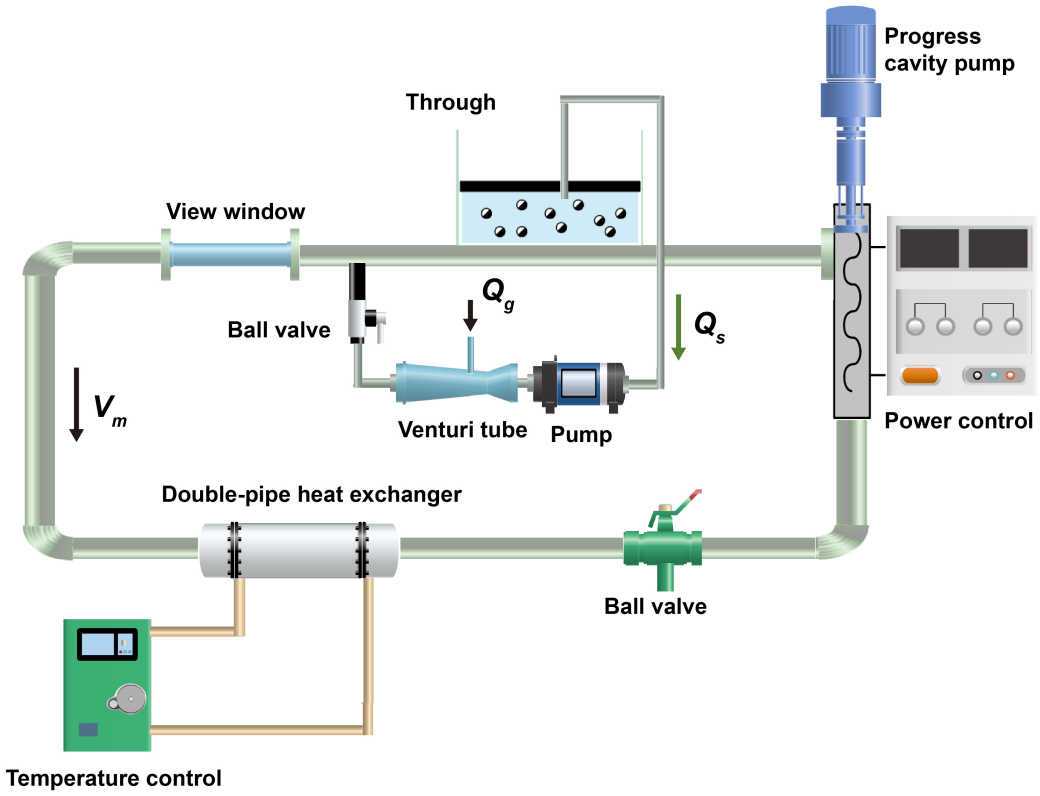

(a)

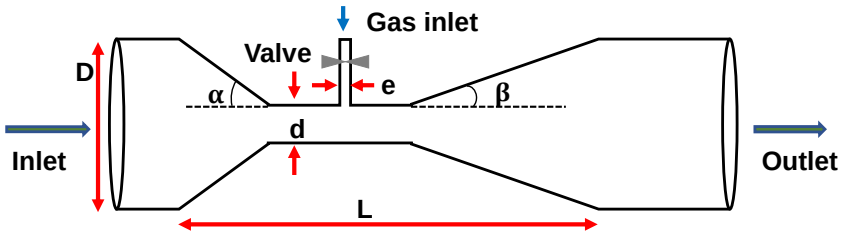

(b)

Figure 1: (a) Schematic of the lab-scale pipeline loop with the microbubble injection at the upstream of the trough.[10,37] (b) Schematic of the modified venturi tube. Design parameters: D = 9.7 mm, d = 3 mm, L = 26 mm, e = 2 mm, $\alpha = 15$, $\beta = 30$. V_m: slurry velocity in the main loop; Q_s: slurry flow rate in the side stream into the venturi tube; Q_w: flow rate of the circulating water to the heat exchanger; Q_g: gas flow rate into the venturi tube.

ball valve was to drain the waste fluid at the end of the process.

2.2 Dimensions of the Venturi Tube

The design of the Venturi tube (Figure 1(b)) was based on an optimal design with an opening,[10] which generates bubbles by hydrodynamic cavitation based on the Bernoulli principle. A hole was made at the throat section, allowing continuous gas suction at that specific location due to a pressure drop. The gas suction increases bubble production significantly and produces more small bubbles than classic cavitation. Our previous work showed significant improvements in bubble–assisted bitumen recovery from tailings with similar venturi designs.[10]

2.3 Preparation of Artificial Oil Sand Tailings

Artificial oil sand tailings were prepared according to an established procedure reported.[10] The dry sand (from Sil Industry Mineral) was first partially hydrated with 7 % of the total process water content. The hydrated sand was rigorously mixed using a power driller for 10 minutes to ensure every sand particle was hydrated. Subsequently, 0.2 wt% of preheated bitumen at 80 °C was added to wet sand. The bitumen was first partially stirred into the wet sand by hand for 5 minutes to ensure no bitumen would stick to the mixing vessel when mixed with the power drill for an additional 10 minutes. The remaining 93 % of the total process water was added to the sand mixture and was carefully mixed to ensure no air bubbles were entrained. The composition of artificial tailing and the properties of process water are listed in Table1.

2.4 Heating Process of Tailing Slurry in Hydrotransport Loop

At first, the pipeline was preheated with circulating tap water to reduce the time needed to heat the artificial tailings after their preparation. When the artificial tailings are prepared, the tap water in the loop is completely discharged, and 7.8 kg of artificial tailing is added instantly to the loop. The artificial tailing is heated for approximately 20 to 30 minutes

Table 1: Physical properties of water and artificial tailing composition.[42]

Parameter	Value
Artificial tailing	
Solid (wt%)	50
Process water (wt%)	49.8
Bitumen (wt%)	0.2
Process water properties[10]	
pH	7.5
Surface tension (mN/m)	70.1
Chemical composition	Calcium, ammonia, magnesium, sodium, bicarbonate, chloride, sulfate

before reaching an equilibrium set temperature.

2.5 Characterization of Microbubbles

Focused beam reflectance measurement (FBRM G400, Mettler Toledo) was applied to measure the real-time size and number of generated microbubbles by venturi tube under the applied conditions for bitumen recovery. A rotating lens focuses the laser beam into the dispersed medium at a speed of 2 m/s through a sapphire window. The exposed laser beam rapidly scans the suspended objects close to the sapphire window. The backward light scattering due to hitting the edge of the suspended object is detected and analyzed to obtain the elapsed time for the laser beam to cross the two edges of the object. FBRM allows the characterization of bubble populations ranging from 0.5 to 1000 μm. The bubble size's chord length can be calculated with the laser beam's available elapsed time and speed. Further details on the working principle of FBRM readers can refer to our previous works.[10,33] It should be noted that the measured chord length by FBRM is smaller than the real diameter of microbubbles. In addition, this technique cannot distinguish different particles. The characteristics of microbubbles were just conducted in the clean process water.

2.6 Injection of Microbubbles

As shown in Figure 1, microbubbles were injected upstream of the trough. The artificial tailing in the trough was pumped through the venturi tube by a peristaltic pump to generate microbubbles by cavitation and air suction from the atmosphere and transported back to the pipeline loop through the top ball valve. To generate CO_2 microbubbles, CO_2 gas cylinder was connected to the gas inlet of the venturi tube. Various CO_2 flow rates can be studied by adjusting the outlet pressure of the gas cylinder.

2.7 Froth Collection and Determination of Bitumen Recovery

A large number of microbubbles were coupled with liberated bitumen and solids. The flotation of microbubbles carried particles to the trough and formed a froth containing solids, bitumen and process water. The froth collection was conducted at four–time intervals to determine bitumen recovery with increasing time. Eventually, collected froth samples were transferred to Dean Stark to measure the recovered weight of bitumen, water and solids.

In this work, all experiments are repeated three times to confirm the reproducibility and identify the effect of variables. Operating parameters are summarized in Table 2. The obtained results regarding bitumen recovery with time to be introduced next were fitted to a first–order disappearance kinetic model shown below to evaluate overall bitumen recovery kinetics.[43]

$$R = \mathrm{R}_\infty(1 - e^{-kt}) \tag{2}$$

where R and R_∞ represent the bitumen recovery at time t and infinite respectively, and k is the bitumen flotation rate constant (min^{-1}).

Table 2: Experimental operating conditions of hydrotransport pipeline loop.

Flow velocity in the pipeline loop (m/s)	Flow rate through the venturi tube (L/min)	Gas	Temperature (°C)	Gas flow rate (L/min)
2.0	6.5	CO_2	47	1.4; 1.6; 3.2
		Air	42	0; 1.4
		Air	30; 47; 52	1.4
	8.6	Air	42	0
2.5	6.5	Air	42	1.4

3 Results and Discussion

3.1 Characteristics of Microbubbles in Process Water

This section systematically investigated microbubble formation through hydrodynamic cavitation. The photos of process water with bubbles are displayed in Figure 2(a). From cavitation with air or CO_2 suction, the milky process water contained a larger number of macrobubbles. As comparison, the process water was less milky only a few macrobubbles from cavitation without gas suction.

For various conditions using the FBRM technique, the number of bubbles and bubble size distribution was analyzed in solid-free process water. The FBRM probe recorded the instantaneous distribution of bubble size and number of microbubbles for every 2 seconds. As represented in Figure 2(b) for 30 °C and the airflow rate of 0.4 L/min and liquid flow rate of 6.5 L/min, the number of bubbles reached the peak of bubble number after 4 s. The majority of bubbles are <10 μm. The number for bubbles larger than 30 μm dropped rapidly. With time, the bubble number and size distribution had negligible change, and the total number of microbubbles reamined relatively constant.

Microbubbles (<10 μm) at 20 seconds are shown in Figure 2(c)-(g). With air suction from the atmosphere at airflow rate of 0.4 L/min and liquid flow rate of 6.5 L/min, the number of microbubbles ranged from $2,000$ to $5,000$ at 20 s for temperatures ranging from 30 °C to 52 °C. The slight difference in the bubble number is not highly associated with the temperatures in the clean process water. However, fewer microbubbles were produced at 47

°C compared to the other temperatures. It should be noted that the previous study of Xu et al.[44] also reported the probability of nanobubble formation from gas oversuated in water was minimal at temperature around 45 °C compared to lower or higher temperatures. The low probability of bubble formation may be related to the non-monotonic dependence of gas solubility on the temperature of water, which was also reflected in bubble formation on solid substrates.[44,45] Furthermore, with suction of CO_2 from 0.4 L/min to 3.2 L/min, the bubble number increased rapidly in the first 6 seconds and reached 4,000-8,000, and then increased gradually with time when the flow was 6.5 L/min at 47 °C. There were the large fluctuations in bubble number with time.

The results obtained from air and CO_2 flow rate were compared at a fixed liquid flow rate of 6.5 L/min and temperature of 47 °C. The differences in number and stability of microbubbles from suction of air and CO_2 injection may be related to the higher solubility of the former in water. The amount of dissolved CO_2 significantly increased with time in the beginning until the process water was saturated with CO_2. The high concentration of dissolved CO_2 aided the stabilization of produced microbubbles.[46] On the other hand, the air showed a relatively low solubility and contributed to a flatter trend of growing microbubble number.

The effect of cavitation without gas suction was also examined. Figure 2(f) indicates that at 42 °C the bubble number increased steadily with time. At the liquid flow rate was 6.5 L/min or 8.6 L/min, there was insignificant difference in the number of bubbles at given time of cavitation. At the identical liquid flow rate of 6.5 L/min and temperature of 42 °C, the cavitation effect produced a similar number of microbubbles as air suction at 0.4 L/min as shown in Figure 2(g). However, the cavitation stimulated microbubbles were mainly comprised of vapor bubbles, so their lifetime is expected to be short at the experiment temperature of 42 °C. In the measurements by FBRM, the probe detects the bubbles nearby. Presence of a few large bubbles near the probe may lead to a lower number density of recorded microbubbles, which may attribute to the fluctuation of the bubble numbers measured in

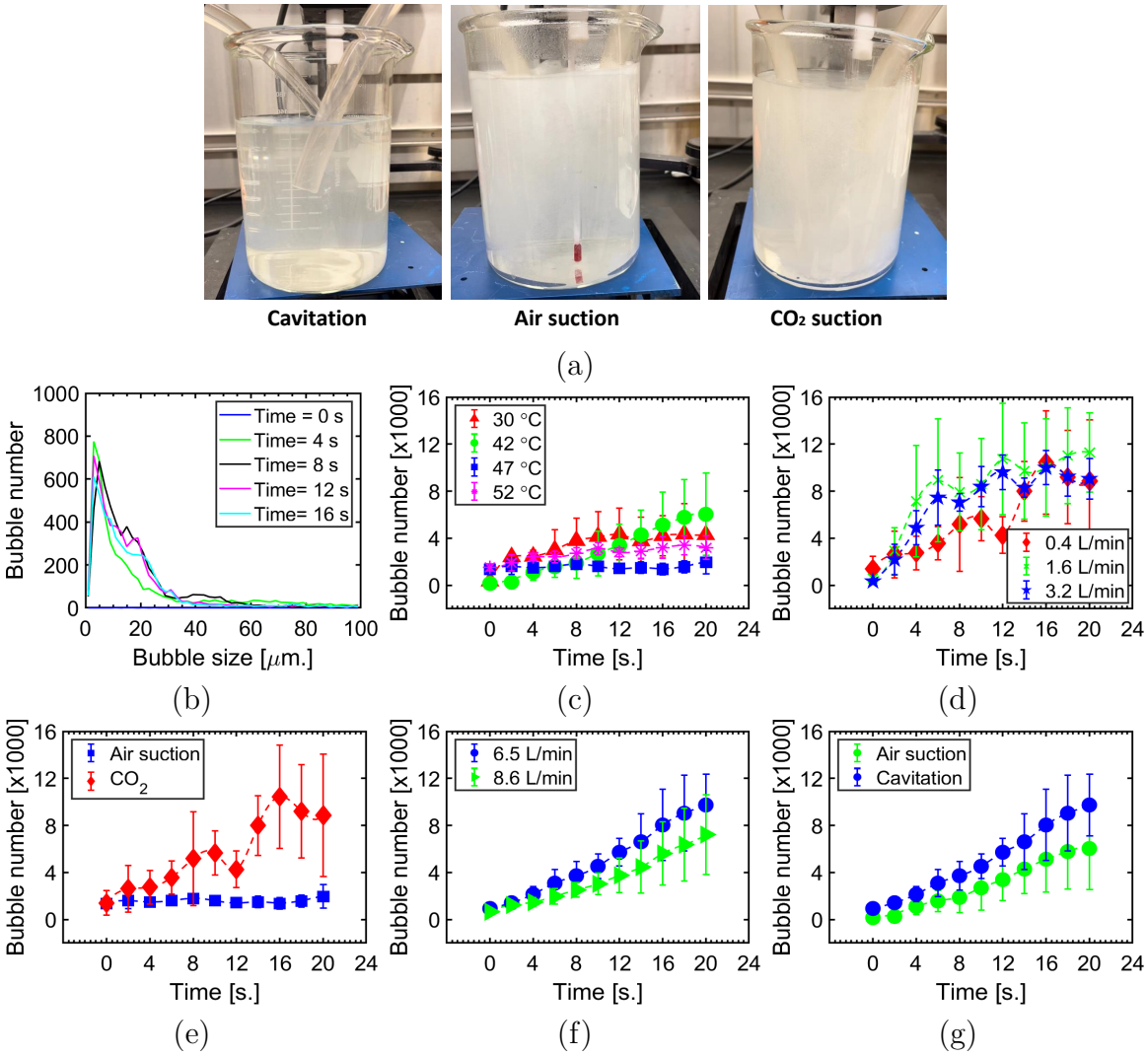

Figure 2: Images of produced microbubbles in the process water: (a) (consistent liquid flow rate: 6.5 L/min) Cavitation: Gas flow rate: 0 L/min, at 42 °C; Air suction: Gas flow rate: 0.4 L/min, at 42 °C; CO_2 suction: Gas flow rate: 0.4 L/min, at 47 °C. Bubble size distribution *vs* time: (b) Air flow rate: 0.4 L/min; Liquid flow rate: 6.5 L/min, at T: 30 °C; Bubble (<10 μm) number *vs* time: (c) Air flow rate: 0.4 L/min; Liquid flow rate: 6.5 L/min, at T: 30 °C, 42 °C, 47 °C, and 52 °C; (d) CO_2 flow rate: 0.4 L/min, 1.6 L/min, 3.2 L/min; Liquid flow rate: 6.5 L/min, at T: 47 °C; (e) CO_2/Air flow rate: 0.4 L/min; Liquid flow rate: 6.5 L/min, at T: 47 °C; (f) Air flow rate: 0 L/min; Liquid flow rate: 6.5 L/min, 8.6 L/min ,at T: 42 °C; (g) Air flow rate: 0 L/min, 0.4 L/min; Liquid flow rate: 6.5 L/min; T: 42 °C.

different run.

The results from the FBRM technology in this section provide characteristics of bubble numbers and size under several operating conditions in bubble generation by venturi tube in

process water. Although FBRM can not offer the ability to analyze the bubbles in the highly concentrated tailing slurry quantitatively, this methodical study will provide some valuable insight into the role of microbubbles in recovering bitumen from artificial tailings in the loop in the following sections.

3.2 Enhanced Bitumen Recovery from Highly Concentrated Tailing Slurry

The oil sand tailings consist of sands, silts, clays, process water, unrecovered hydrocarbons and other contaminants. Typically, the discharged oil sand tailings from the primary separation vessel are concentrated with 60–70 % solids.[3] The amount of residual bitumen trapped in the oil sand tailings ranges from 0.5–3 wt%, depending on the processing procedure.[3] In the present study, the bitumen recovery from highly concentrated artificial oil sand tailings with 50 wt% of solid composition with and without microbubbles was systematically studied. Figure 3(a) illustrates the bitumen recovery at a constant slurry flow velocity of 2 m/s and temperature of 42 °C. The result revealed that the bitumen recovery of 39 % was obtained at 32 min without the injection of microbubbles.

The recovered bitumen was slightly higher for collected samples with the injection of microbubbles, as shown in Figure 4(b1). The enhanced bitumen recovery was 34 % at 8 $mint$ and increased up to 51 % at 32 min. The application of microbubbles was advantageous to the bitumen separation from the tailing slurry. This observation is in accordance with a previous study in the literature on bitumen separation from a slurry with microbubbles for a much lower solid composition of 6.62 %.[10] All conditions were consistent for comparison, except a higher temperature in this study as shown in Table 3. The highly concentrated slurries obtained a similar magnitude of bitumen composition with increased solid composition and decreased water composition. Therefore, the injection of microbubbles to the slurry flow substantially impacts bitumen recovery for the oil sand tailings of high solid contents.

Figure 3(b1),(b2) shows the experimental observation of recovered froth in the trough at

Table 3: Comparison of Bitumen Separation Conditions.

Parameter	Bitumen (wt%)	Solid (wt%)	Water (wt%)	Q_g (L/min)	Q_s (L/min)	V_m (m/s)	T (°C)
Present study	0.2	50	49.8	1.4	6.5	2	42
Dashliborun et al[10]	0.2	6.62	93.18	uncontrolled	6.5	2	40

different time intervals where sampling started. From Figure 3(b1), a thick froth layer that contained dark bitumen, solids, tiny bubbles and water were observed when microbubbles were injected. In contrast, a small number of scattered bitumen droplets was floated on the surface from 8 min to 24 min, as shown in Figure 3(b2).

Furthermore, to better understand the effect of microbubbles on the froth quality, the composition of the collected froth layer was analyzed by the Dean–Stark apparatus to determine the weight fractions of bitumen, solids and water. Figure 4 shows the results from the composition analysis of froth at the same experimental operating conditions. The collected bitumen composition was relatively small compared to the water and solid compositions, as shown in Figure 4(a1),(a3). The composition of solids grows modestly with increased time ranging from 20 % to 40 % (Figure 4(a2)). The quality of froth and solid composition without microbubbles appeared to be higher due to the smaller amount of water. Additionally, the mass of solids and water in the froths was twice when microbubbles were injected, as shown in Figure 4(b2),(b3). It agrees well with the phenomenon that thick layers composed of a large amount of water and solids appeared in all intervals in Figure 3(b1),(b2). This finding highlights that air bubbles improved bitumen recovery from the tailings of high solid content, although the froth contained water and solids.

The venturi tube allowed air suction at the neck due to pressure reduction. The air stream was sheared by hydrodynamic flow and thus produced more air bubbles in addition to vapor bubbles. As shown in Figure 3(a), it is evident that the bitumen recovery with air addition outperformed the operation without air addition. The long persistence time of microbubbles facilitated sufficient interactions between bitumen droplets and bubbles in the flow. The high surface–to–volume ratio and internal pressure of microbubbles could improve

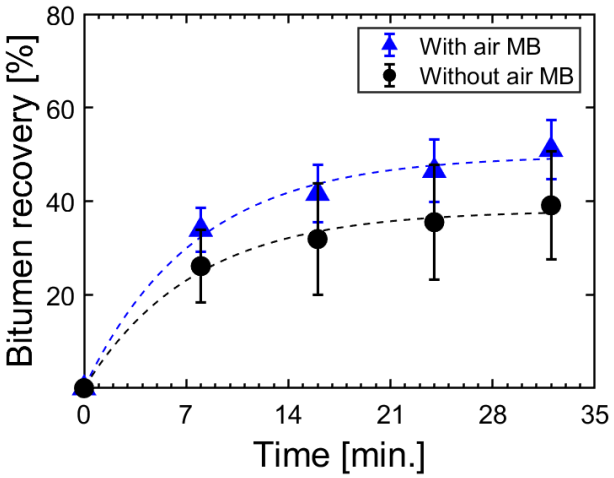

(a)

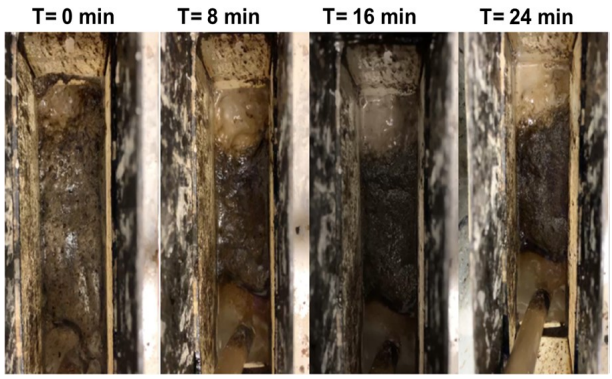

(b1)

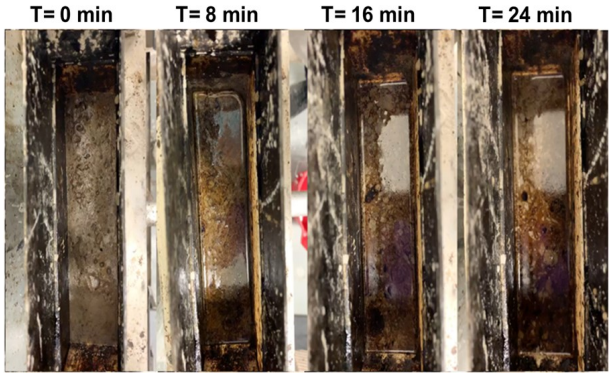

(b2)

Figure 3: Effect of air MBs on bitumen recovery: (a) plot of bitumen recovery versus time. Photos of recovered froth layer: (b1) with air addition; (b2) without air addition, at V_m: 2 m/s; T: 42 °C; Q_s: 6.5 L/min; Q_g: 1.4 L/min.

the probability of collision between bubbles and bitumen and shorten the induction time before attachment. Additionally, the highly concentrated hydrodynamic flow could increase bubbles' break–up and hinder the coalescence of bubbles, which is also beneficial for bitumen

separation.[47] The aggregates of bitumen with the aid of bubbles have a lower density and are separate from the slurry.

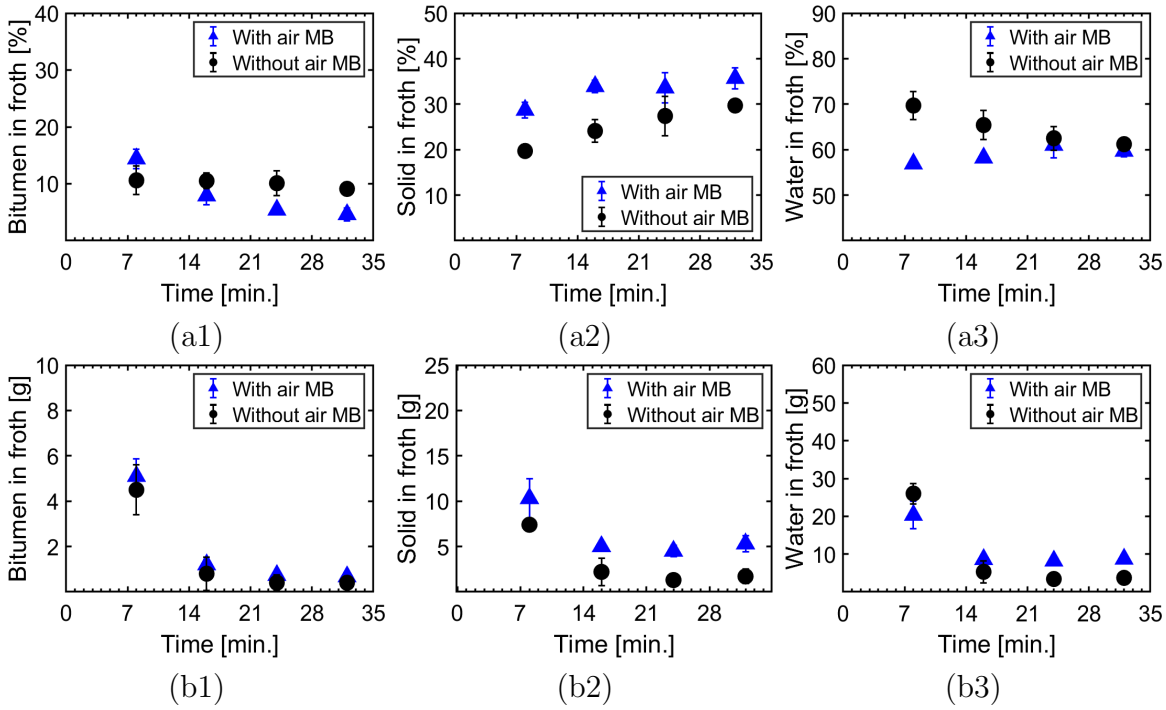

Figure 4: Composition of the collected froths: (a1) bitumen; (a2) solid; and (a3) water. Weight of recovered impurities at time intervals: (b1) bitumen; (b2) solid; (b3) water, at V_m: 2 m/s; T: 42 °C; Q_s: 6.5 L/min; Q_g: 1.4 L/min.

Air bubbles are efficient for recovering bitumen, especially at lower temperatures. The cumulative bitumen recovery was increased by 10 % due to the addition of air bubbles at 42 °C (Figure 3(a)). However, the injection of air bubbles is not advantageous for recovering bitumen at high temperatures, which will be discussed in the later section.

3.3 Effect of Cavitation

The production of air bubbles in the previous section was the multiple effects of air suction through the gas inlet of the venturi and cavitation due to pressure drop at the throat. This section used only the cavitation effect by fully plugging the gas inlet at 42 °C and the slurry flow velocity in the pipeline of 2 m/s. In addition to the initial side stream flow rate of 6.5 L/min through the venturi tube, the higher side stream flow rate of 8.6 L/min was also

studied. Figure 5 shows that the bitumen recovery of 30 % was obtained at the side stream flow rate of 6.5 L/min, which was even lower than the bitumen recovery of 40 % (Figure 3a). The recovery efficiency was increased to 50 % as the side stream flow rate was increased to 8.6 L/min. It can be ascribed to a large amount of recovered bitumen within the first 16 minutes (Figure 6(b1)). The higher side stream flow rate through the venturi tube was improved the bitumen recovery significantly, as much as the overall bitumen recovery at the side stream flow rate of 6.5 L/min with air suction.

The composition of bitumen increased rapidly from 8 min to 24 min and decreased as shown in Figure 6(a1). The quality of froths with cavitation is better with a small amount of recovered solids and water (Figure 6(b2),(b3)). The composition of water revealed the inverse trend compared to bitumen (Figure 6(a2)). A relatively high water composition above 70 wt% was observed at 8 min, but it decreased below 60 wt% from 24 min to 32 min. Besides, the composition of solids was lower with intensified cavitation, while the composition of water was the same (Figure 6(a3)). The results reveal the pros and cons of air suction: High bitumen recovery could be reached with air suction at the lower flow rate in the venturi tube, although the froth quality was lower. Better froth quality could be obtained by cavitation without air suction. However, more kinetic energy was required to create a faster flow through the venturi tube without the air suction.

Many researchers have studied the separation of organic materials by adding bubbles.[37,43] Bubbles have a strong affinity for hydrophobic oil droplets. The aggregates formed by bubbles and bitumen are light in density, accelerating the separation of bitumen from the slurry.

According to the Bernoulli principle, as the pressure at the throat falls below the saturated vapor pressure, water vaporizes to bubbles.[30,33] The cavitation strength is determined by the pressure ratio of downstream pressure to upstream pressure of the venturi tube.[48] As the pressure ratio decreases, more small vapor bubbles and air bubbles can be formed theoretically due to the intensified cavitation. At a higher side stream flow rate through the venturi tube, the pressure ratio decreased with increasing the upstream pressure. Besides,

a more vital turbulent interaction between slurry and gas in the divergent section decreases the bubble size effectively.[49] However, vapor bubbles accounted for a significant fraction of produced microbubbles. The collapse of vapor bubbles was strengthened in the more turbulent conditions.[50] As shown in Figure 2(d), similar number of microbubbles were detected for both liquid flow rate in the clean process water. However, the presence of solids in the process water significantly influenced the cavitation. Particle with rough surfaces brings gas pockets to the slurry and stabilizes the gas nuclei in the liquid. Consequently, the solids in the process water can promote the hydrodynamic cavitation notably.[51] On the other hand, when the slurry flow rate in the side stream was increased to 8.6 L/min, the more hydrodynamic slurry stream was injected into the pipeline loop. This implies an increase in turbulence flow of the oil sand tailings in the loop, enhancing the dispersion of minerals and bitumen droplets. The higher bitumen recovery might be attributed to the intensified turbulence.

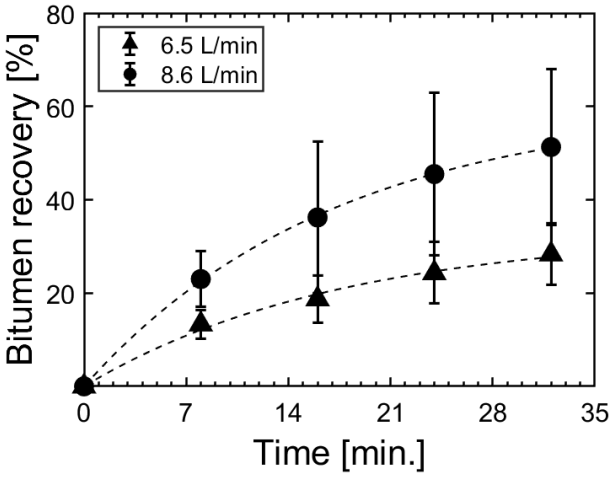

Figure 5: Effect of side stream flow rate on bitumen recovery without gas injection for Q_s: 6.5 L/min, 8.6 L/min, at T: 42 °C; V_m: 2 m/s; Q_g: 0 L/min.

3.4 Effect of CO_2 Microbubbles on Bitumen Recovery

To demonstrate the role of CO_2 bubbles in recovering bitumen from oil sand tailings, CO_2 was injected into the gas inlet of the venturi tube at three different gas flow rates. First of all, at 47 °C and the slurry flow velocity of 2 m/s, the carbon dioxide was injected at 1.4 L/min,

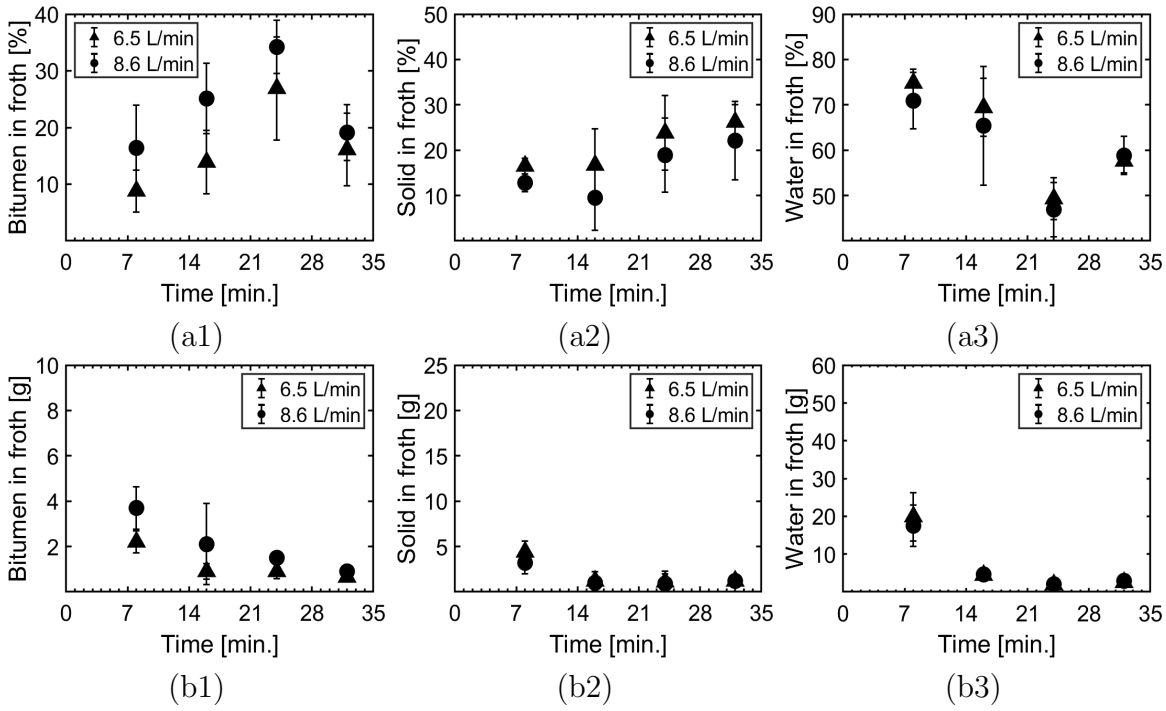

Figure 6: Composition of the collected froths: (a1) bitumen, (a2) solid, and (a3) water; Weight of recovered impurities at time intervals: (b1) bitumen; (b2) solid; (b3) water, at Q_s: 6.5 L/min, 8.6 L/min; T: 42 °C; V_m: 2 m/s; Q_g: 0 L/min.

the same as the airflow rate in section 3.2. Moreover, a gas–washing bottle was applied to keep the atmospheric pressure at the gas inlet. In this case, the bitumen recovery was 50 % shown in Figure 7(a). Interestingly, from the trough, thicker froths carrying massive bubbles and solids with CO_2 injection were observed, compared to froths with air injection as shown in Figure 7(b1),(b2).

When the CO_2 flow rate was increased to 1.6 L/min and 3.2 L/min, CO_2 was directly pressurized into the gas inlet from the gas cylinder. Interestingly, the bitumen recovery was increased to 61 % with an increased CO_2 flow rate to 1.6 L/min (Figure 7(a)). Nevertheless, the bitumen recovery decreased from 61 % to 50 % for high CO_2 flow rate of 3.2 L/min, which indicates that the higher gas flow rate is not beneficial to recovering bitumen from the oil sand tailings. It agrees well with the results in Figure 8(b1). The injected CO_2 made no improvement in the quality of froth (Figure 8(a1)). The total compositions of water and solids occupied even above 90 % for all collected samples. The compositions of water and

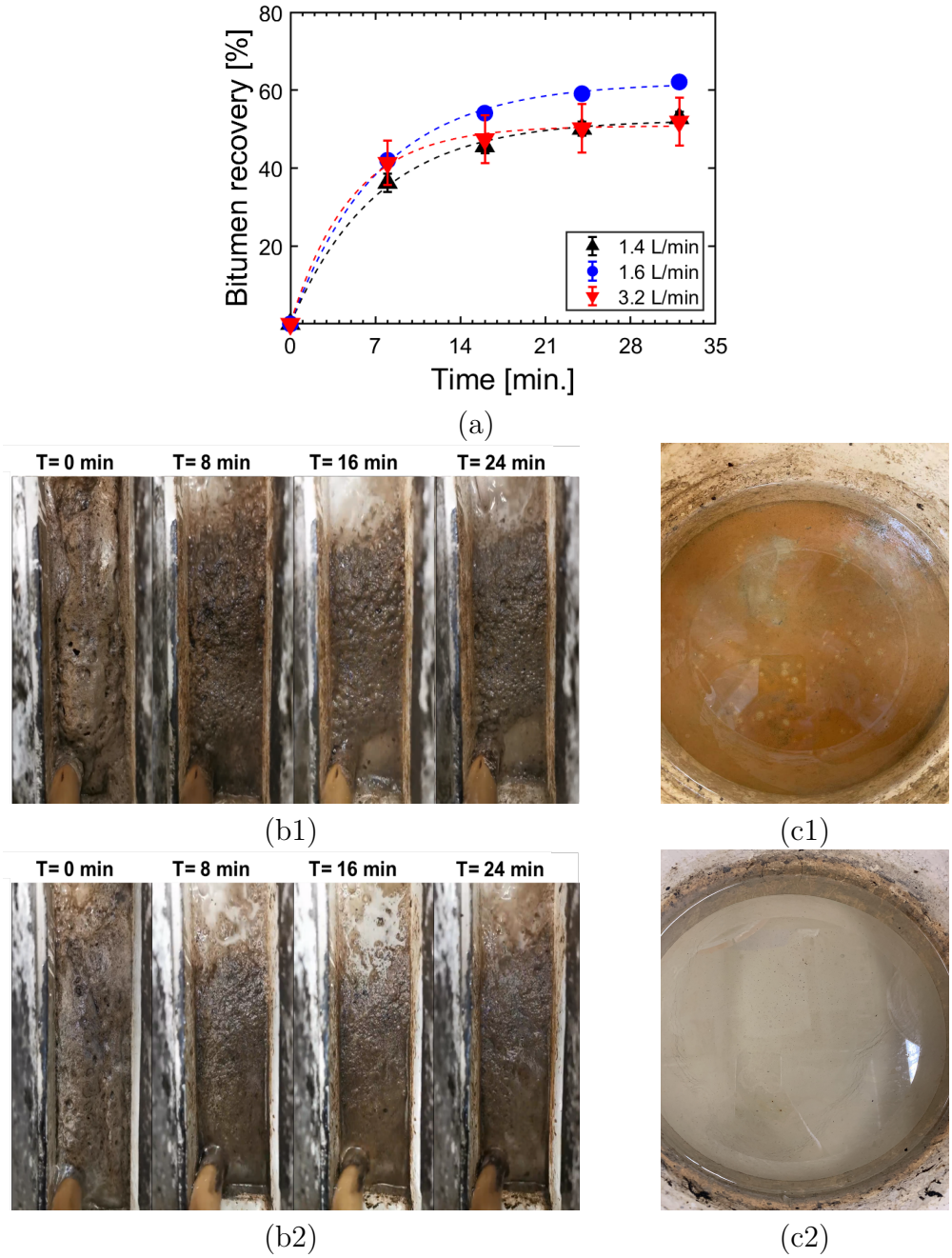

Figure 7: (a) Effect of CO_2 addition on bitumen recovery. Experimental observations of recovered froth layer at four time intervals: (b1) with CO_2 addition; (b2) with air addition; Experimental observations of deposited tailing wastes: (c1) with CO_2 addition; (c2) with air addition, at V_m: 2 m/s; T: 47 °C; Q_s: 6.5 L/min; Q_g: 1.4 L/min.

solids fluctuated near 70 % and 30 % respectively (Figure 8(a2),(a3),(b2),(b3)).

In addition, the surface of deposited solids after discharge presented different colors with CO_2 and air injection. As shown in Figure 7(c1), the deposited solids showed the original

color of sands with air injection. It is quite different from the observation that a layer of red fines sedimentation was formed on the top of sands with CO_2 injection (Figure 7(c2)). The sand samples and process water contains metallic compositions in the form of oxides. For the appearance of fine red particles in the tailing suspension, it might be result from the reaction of metallic compositions with CO_2, and enhanced flotation of metallic compositions by CO_2 bubbles. However, a further study is required to characterize the chemical composition of red fines and understand the mechanism of the phenomenon with CO_2.

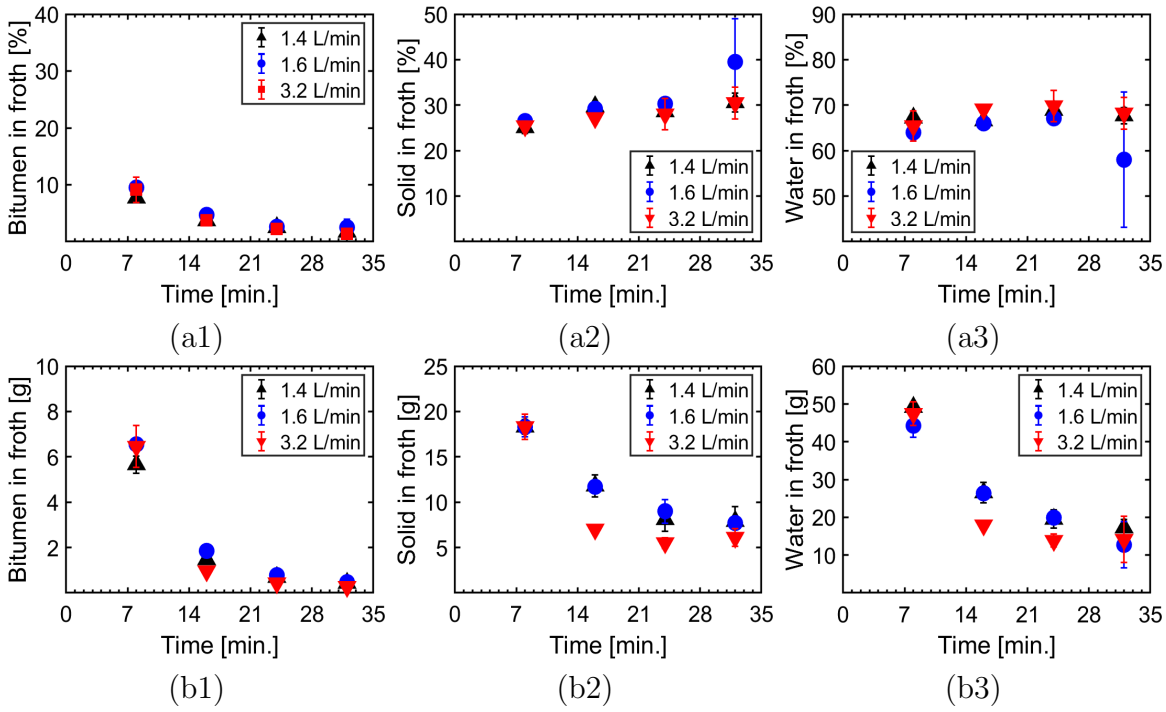

Figure 8: Composition of the collected froths: (a1) bitumen, (a2) solid, and (a3) water; Weight of recovered impurities at time intervals: (b1) bitumen; (b2) solid; (b3) water, at Q_g: 1.4 L/min, 1.6 L/min, 3.2 L/min; V_m: 2 m/s. Q_s: 6.5 L/min. T: 47 °C.

Similar to the injection of air, injected CO_2 was sheared into tiny bubbles at the divergent section by turbulent flow. The difference is that CO_2 is well known for its high solubility. With decreasing pressure or increasing temperature, dissolved CO_2 nucleates on hydrophobic surfaces and grows.[35] The dissolved CO_2 also helps stabilize the vapor bubbles produced by the cavitation effect. Despite the high solubility, the dissolved CO_2 decreased the pH of a solution. The acidic environment inhibited the release of natural surfactant from

bitumen to deteriorate the interaction between bubbles and bitumen.[40] A larger number of microbubbles were observed with the injection of CO_2 in the clean process water (Figure 2(c)). However, it is found that the bitumen recovery through CO_2 injection was similar to that with air injection at the same operating conditions as shown in Figure 7(a). In the artificial tailing slurry, the mineral solids can react with dissolved CO_2 that is disadvantageous to the microbubble production.

Figure 2(b) showed that the CO_2 flow rate made little difference to the bubble number. It should be noted that the gas holdup differs a lot for the various volume of tested liquid when the gas is injected at the same flow rate. The gas hold up plays an important role in bubble production. As the CO_2 flow rate increased for the tailing slurry, more dissolved CO_2 was added. The dissolved CO_2 not only enhance the stabilization of vapor bubbles by transfer into those vapor bubbles but also restrain the CO_2 molecules diffusion into the liquid. Thus, a higher amount of vapor bubbles and CO_2 bubbles can reside for a longer time in the process water with more dissolved gas.[30] Additionally, more CO_2 bubbles were generated by shear force cavitation–induced nucleation at a higher CO_2 flow rate. Hence, the bitumen recovery was improved at the CO_2 flow rate of 1.6 L/min. However, the bitumen recovery returned to 50 % when the CO_2 flow rate was increased to 3.2 L/min. The previous literature demonstrates that the higher CO_2 holdup is adverse to generate tiny bubbles because large bubbles escape from shearing behavior at the divergent section.[49] As well, the significant CO_2 holdup accelerates the coalescence of bubbles.

3.5 Effect of Flow Velocity

In this section, the flow was circulated at 42 °C with the slurry flow velocity increased from 2 m/s to 2.5 m/s in the pipeline loop. As seen from Figure 8, the bitumen recovery of 50 % was obtained within 32 minutes with air addition at the slurry flow velocity of 2.5 m/s. However, with increasing the slurry flow velocity to 2.5 m/s when air bubbles were injected, bitumen recovery efficiency was negligible. Figure 10(a1)(b1) shows that bitumen

was mainly recovered in the first 8 minutes. The compositions of solids and water in the froth were in the range of 20 % to 35 % and 50 % to 65 % separately (Figure 10(a2)(a3)). In addition, the recovered water was approximate twice the recovered solids as well (Figure 10(b2)(b3)).

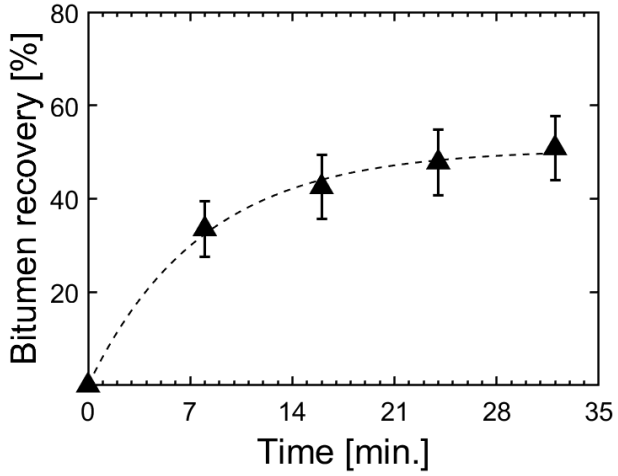

Figure 9: Effect of flow velocity on bitumen recovery with air addition, at V_m: 2.5 m/s; Q_s: 6.5 L/min; T: 42 °C; Q_g: 1.4 L/min.

Flow velocity is highly influential to the flow regime of tailing slurry in the transport pipelines. In our experiments, the tailing slurry contains 50 wt% solids composed of 80 % coarse particles with a diameter larger than 44 μm. Coarse particles settle down quickly due to the gravitational effect.[12] A significant fraction of coarse particles leads to heterogeneity of a slurry flow and might cause the formation of a solid bed that possibly restricts the motion of bitumen droplets and contact with bubbles in the tailing slurry. A higher flow velocity with intensified turbulent energy decreases the asymmetry degree of solid concentration in the vertical plane. Moreover, bitumen droplets moved with high kinetic by intensified turbulent flow instead of being trapped in the bed. In the presence of microbubbles, there is no further improvement in the bitumen recovery at a higher flow velocity. For a highly concentrated oil sand tailing slurry, attrition and friction between neighbouring solids and bitumen–bubble aggregates destabilize the attachment between bitumen and bubbles. The bitumen detachment from bubbles was strengthened in the more hydrodynamic tailing slurry.

In addition, the intensified turbulence enhanced the collapse of vapor bubbles produced by cavitation.[46,50]

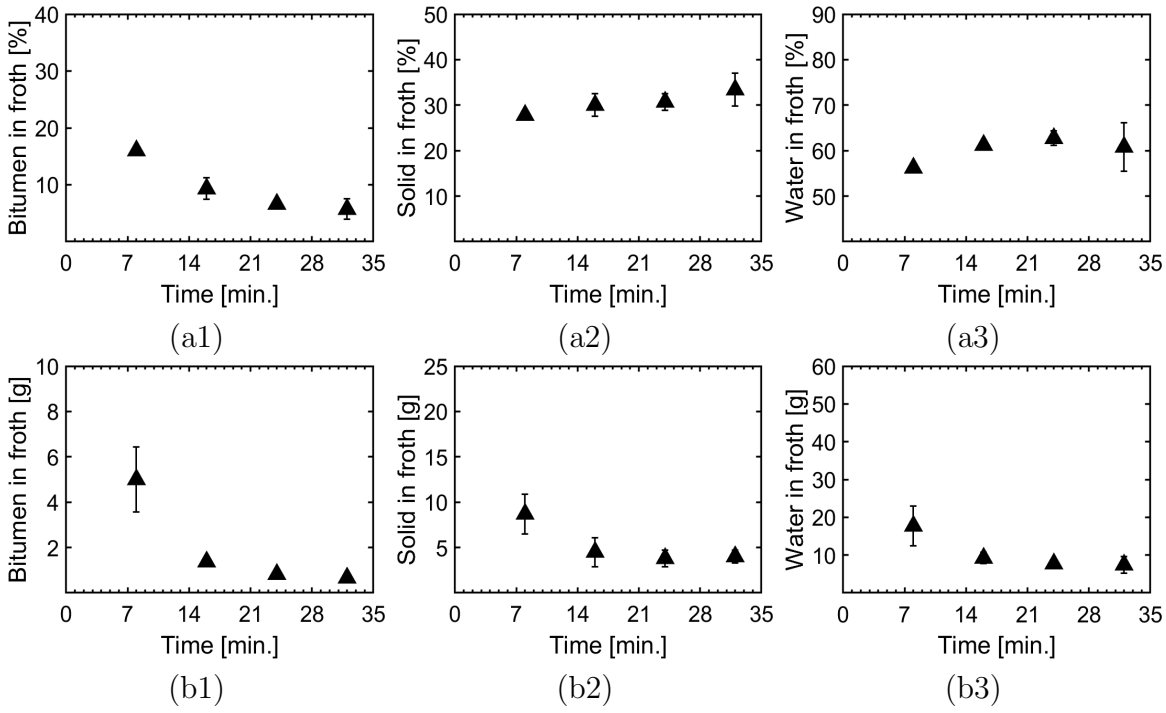

Figure 10: Composition of the collected froths: (a1) bitumen, (a2) solid, and (a3) water; Weight of recovered impurities at time intervals: (b1) bitumen; (b2) solid; (b3) water, at V_m: 2.5 m/s; Q_s: 6.5 L/min; T: 42 °C; Q_g: 1.4 L/min.

3.6 Effect of the Slurry Temperature

Temperature plays a vital role in recovering bitumen from the slurries by influencing the properties of bitumen, such as viscosity and density, and the kinetics of particles which has a significant interaction between particles. Figure 11 displays the cumulative bitumen recovery at the temperatures of 30 °C, 47 °C and 52 °C, respectively, with tailing streams circulated at 2 m/s. A significant enhancement of bitumen recovery was observed with increasing the processing temperature from 30 °C to 47 °C. The bitumen recovery of 37 % at 30 °C was enhanced up to 50 % at 47 °C. It is obvious that the larger amount of recovered bitumen at 16 min and 24 min at 47 °C (Figure 12(a1)). With further increase in temperature to 52 °C, there was no significant improvement in bitumen recovery. The results can be inferred

that there is a critical temperature between 42 °C and 47 °C for enhancing bitumen recovery without air bubbles.

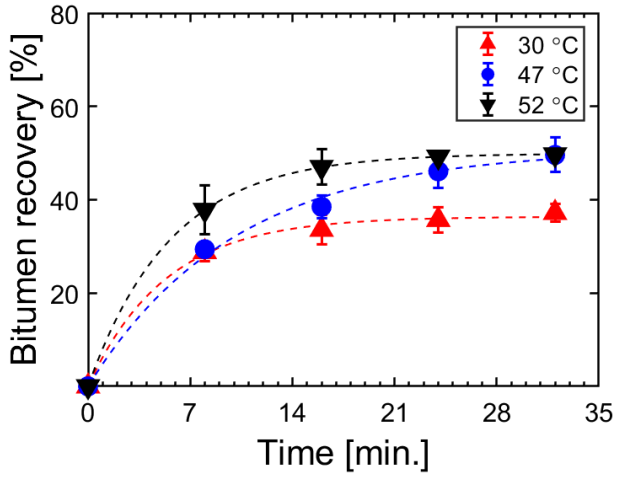

Figure 11: Effect of temperature on bitumen recovery without air addition, at V_m: 2 m/s; T: 30, 47, 52 °C.

As shown in Figure 12(a1), froths collected at 30 °C exhibited poor quality compared with that at 47 °C and 52 °C. It can be attributed to the higher water composition (Figure 12(a3)). The composition of solids at different time intervals followed the same trend and increased with increasing the processing temperature as shown in Figure 12(a2). In accordance with the observation at 42 °C, one can notice that more water and solids were recovered in the first 8 minutes. However, the mass of recovered water and solids decreased rapidly after 8 *min* (Figure 12(b2),(b3)). The temperature has a negligible impact on the recovered amount of solid and water.

Figure 13 demonstrates the influence of temperature on the bitumen recovery when microbubble injection was employed upstream of the trough. The injection of air bubbles increased the relatively low bitumen recovery caused at lower temperatures. Similar increasing bitumen recovery trends at different temperatures were observed with the recovery efficiency of approximate 50 % at 32 *min*. However, the effect of temperature on the bitumen recovery can be distinguished at different time intervals. The higher bitumen recovery of 36 % at 52 °C was seen at 8 *min*. Nevertheless, it was overlapped by the bitumen recovery

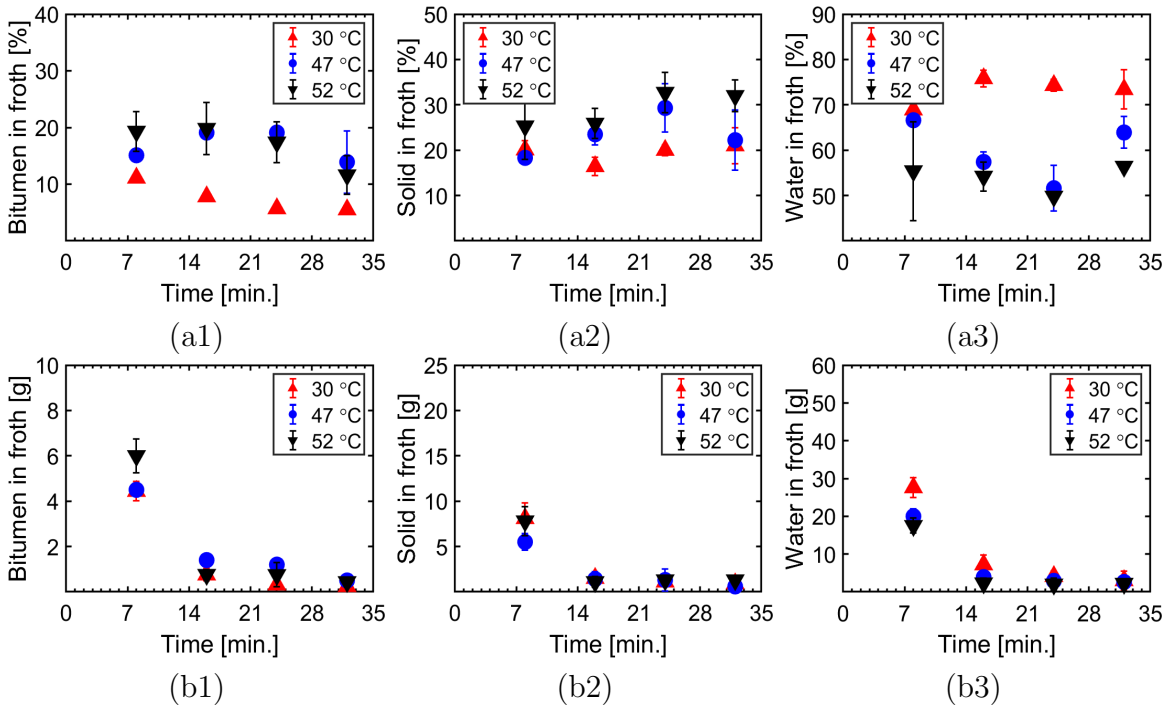

Figure 12: Composition of the collected froths: (a1) bitumen, (a2) solid, and (a3) water; Weight of recovered impurities at time intervals: (b1) bitumen; (b2) solid; (b3) water, at V_m: 2 m/s; T: 30 °C, 47 °C, 52 °C.

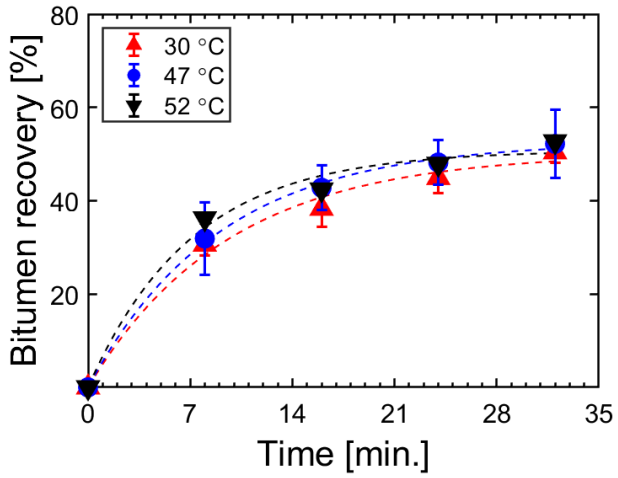

Figure 13: Effect of temperature on bitumen recovery with air addition. V_m: 2 m/s; Q_s: 6.5 L/min; Q_g: 1.4 L/min. T: 30 °C, 47 °C, 52 °C.

at 47 °C since 16 min. The bitumen recovery at 30 °C was slightly lower than the higher temperatures.

The temperature did not influence the quality of froths with bubbles, weight fractions of bitumen decreased rapidly by approximate 5 % firstly and then experienced a slight decline

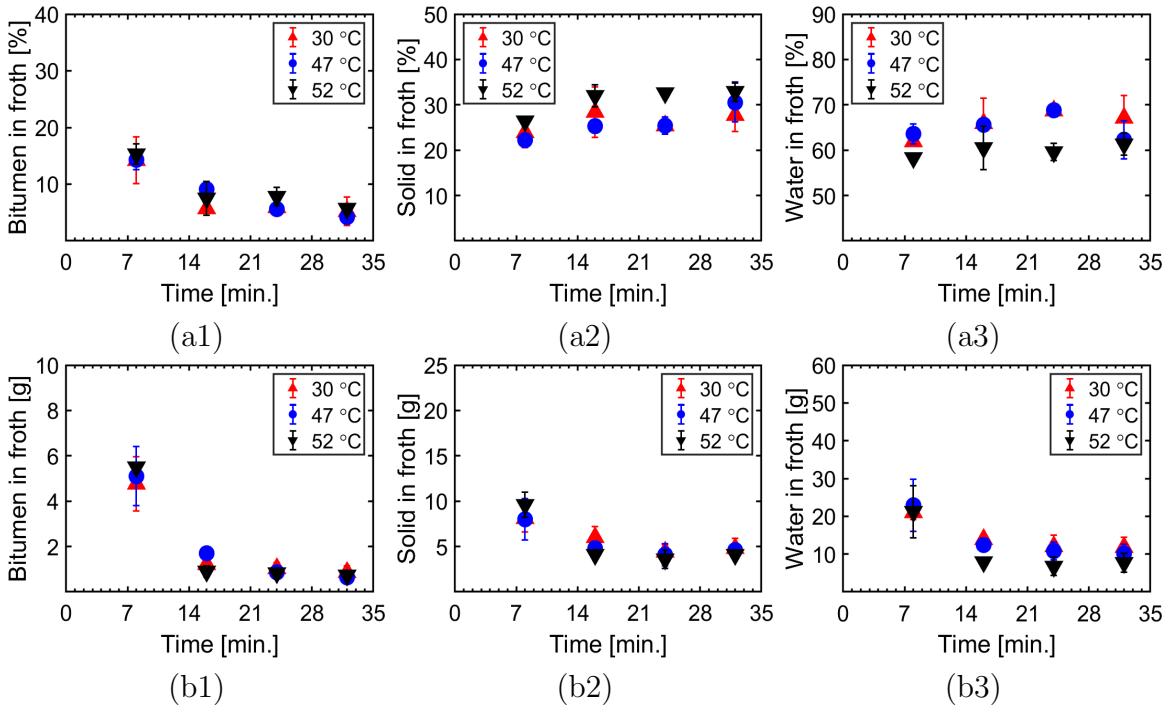

Figure 14: Composition of the collected froths: (a1) bitumen, (a2) solid, and (a3) water; Weight of recovered impurities at time intervals: (b1) bitumen; (b2) solid; (b3) water, at V_m: 2 m/s; Q_s: 6.5 L/min; Q_g: 1.4 L/min. T: 30 °C, 47 °C, 52 °C.

with changing time from 16 *min* to 32 *min* (Figure 14(a1)). It is worth noting that a similar trend as the recovered amount of bitumen (Figure 14(b1). As seen from Figure 12(a1) and 14(a1), the froth quality was similar with and without air addition at 30 °C and 42 °C. However, bubble injection deteriorated the froth quality at 47 °C and 52 °C. The larger amount of recovered bitumen with air bubbles counteracted the larger amount of water and solids. Thus little difference in froth quality was observed at lower temperatures. The addition of air bubbles increased the amount of recovered water and solids in the froth (Figure 12(b2),(b3) and Figure 14(b2),(b3)). However, a similar amount of recovered bitumen in the froths at higher temperatures of 47 °C and 52 °C. Consequently, the lower quality of froths was obtained with air bubbles at high temperatures. The solid composition with air addition grew gently with increasing time ranging from 20 % to 35 % (Figure 14(a2)). The water constituted the largest fraction of froth (Figure 13(a3)).

Much research has been conducted to understand the relationship between temperature

and the properties of bitumen. Viscosity, the density of bitumen, and interfacial tension between water and bitumen that significantly impact bitumen recovery are influenced by temperature.[52–54] In literature, a remarkable decrease in bitumen viscosity is obtained with temperature increasing from 40 °C to 50 °C. As a comparison, bitumen density and interfacial tension decrease a little with increasing the temperature. Schramm[55] pointed out that high bulk viscosity of the fluid decreases the bitumen rise velocity, thus negatively influencing the separation efficiency of bitumen in flotation. Increasing the temperature decreases the viscosity of oil sand tailings, which can be ascribed to attenuated cohesive force between liquid molecules and intensified kinetic energy of particles.[56] Particles of high kinetic energy have a greater probability of collision behavior.

Gas solubility in water decreases with an increase in temperature.[33,40] Besides, high temperature increases the vapor pressure, which is beneficial to generate vapor bubbles due to the pressure differentiation caused by mechanical shearing in the pipeline loop or cavitation. For aggregates formed by bitumen and bubbles, high temperature stabilizes the attachment between bitumen and bubbles by forming bitumen engulfment, which efficiently inhibits detachment. Additionally, high temperature influences the interaction between clays and bitumen.[13,57] The attachment of clays to bitumen called slime coating dramatically prevents bitumen droplets from contacting with bubbles and other bitumen droplets. With increasing temperature, adhesion between clays and bitumen are decreased to be negligible.[13,58] Surface charge of bitumen and clays become more negative at the same time. The improved repulsive force inhibits the attachment between bitumen and clay particles and improves the separation of bitumen.

Interestingly, a small difference is shown in bitumen recovery with air addition at various temperatures in Figure 12. At the given air flow rate of 1.4 L/min, the air addition at 47 °C and 52 °C showed negligible enhancement in bitumen recovery. Much cleared improvement in bitumen recovery was obtained with air addition at 30 °C and 42 °C demonstrated in Section 3.1. Either increasing temperatures or the addition of air bubbles is advantageous

to bitumen recovery. However, the combination of high temperatures and air bubbles did not result in more bitumen recovery from highly concentrated oil sand tailings. Gu et al.[27] reported that high temperature shortens the induction time for bitumen-bubble and bubble–bubble attachment.[27] In other words, high temperature benefits the adhesion between bitumen and bubbles. However, the number of microbubbles decreases simultaneously due to bubble coalescence and expansion, decreasing the probability of bitumen captured by bubbles. According to the findings from Gao et al.[33], a higher amount of microbubbles were generated in the process of water by cavitation and air suction at a lower temperature.[33] Another study points out that the cavitation intensity is weakened at higher temperatures although the cavitation occurs more easily.[39] Although the temperature seems to have a slight impact on bubble production in the clean process water as shown in Figure 2(a), the tailing slurry is more complex compared to the clean process water with the injection of microbubbles at different temperatures.

4 Conclusions

Our experimental data show that microbubbles could improve the recovery of the residual bitumen from tailings with high solid content during hydrotransport in a laboratory–scale pipeline loop. The bitumen recovery was only 39 % without the injection of microbubbles but could reach 51 % after the same duration with an injection of microbubbles. Compared to microbubbles from the cavitation effect alone at a given slurry flow rate, microbubbles formed with air suction into the venturi tube could lead to higher bitumen recovery, which highlights the importance of the gas type in microbubbles in the separation process. Even more significantly, CO_2 outperformed all the conditions mentioned above in bitumen recovery efficiency. The highest bitumen recovery of 61% among all of our experimental conditions was achieved with suction of CO_2 into the venturi tube for bubble formation. Such a highly desirable effect may be associated with bubble characteristics and pH change in presence of

dissolved CO_2. The results indicate that the optimal gas flow rate in suction is necessary for a good performance in generating microbubbles and recovering bitumen. Increasing the temperature of the tailings sped up the bitumen recovery in a short time but did not improve the overall recovery at 32 *min*. To the best of our knowledge, this work appears to be the first time to show microbubble-enhanced bitumen recovery from a flow of highly concentrated artificial tailings. Therefore, our findings are expected to provide a better understanding and practical guidelines for recovering residual bitumen from high solid content tailings.

Acknowledgement

This work was supported by the China Scholarship Council (202008180018), the Institute for Oil Sands Innovation (IOSI) (Project Number IOSI 2019-04 (TA)) and the Natural Science and Engineering Research Council of Canada (NSERC)-Alliance Grant. This research was undertaken, in part, thanks to funding from the Canada Research Chairs Program. The authors are grateful for technical support from IOSI labs, at the University of Alberta.

References

(1) Gray, M.; Xu, Z.; Masliyah, J. Physics in the oil sands of Alberta. *Phys. Today* **2009**, *62*, 31–35.

(2) Kasperski, K. A review of properties and treatment of oil sands tailings. *AOSTRA J. Res.* **1992**, *8*.

(3) Chalaturnyk, R. J.; Don Scott, J.; Özüm, B. Management of oil sands tailings. *Pet. Sci. Technol.* **2002**, *20*, 1025–1046.

(4) Tanna, R. N.; Redman, A. D.; Frank, R. A.; Arciszewski, T. J.; Zubot, W. A.; Wrona, F. J.; Brogly, J. A.; Munkittrick, K. R. Overview of existing science to in-

form oil sands process water release: A technical workshop summary. *Integr. Environ. Assess. Manag.* **2019**, *15*, 519–527.

(5) Carolin, C. F.; Kumar, P. S.; Saravanan, A.; Joshiba, G. J.; Naushad, M. Efficient techniques for the removal of toxic heavy metals from aquatic environment: A review. *J. Environ. Chem. Eng.* **2017**, *5*, 2782–2799.

(6) English, N. J. Sustainable Exploitation and Commercialization of Ultradense Nanobubbles: Reinventing Liquidity. *ACS Sustain. Chem. Eng.* **2022**, *10*, 3383–3386.

(7) Wu, H.; Wang, W.; Huang, Y.; Han, G.; Yang, S.; Su, S.; Sana, H.; Peng, W.; Cao, Y.; Liu, J. Comprehensive evaluation on a prospective precipitation-flotation process for metal-ions removal from wastewater simulants. *J. Hazard. Mater.* **2019**, *371*, 592–602.

(8) Chang, L.; Cao, Y.; Fan, G.; Li, C.; Peng, W. A review of the applications of ion floatation: Wastewater treatment, mineral beneficiation and hydrometallurgy. *RSC Adv.* **2019**, *9*, 20226–20239.

(9) Su, S.; Huang, Y.; Liu, B.; Han, G.; Xue, Y.; Wang, Y. A Feasible Strategy for Deeply Separating Low Concentrations of Molybdenum from Tungstate Solutions with a High-Efficiency Microbubble Floating-Extraction Concept. *ACS Sustain. Chem. Eng.* **2021**, *10*, 146–158.

(10) Motamed Dashliborun, A.; Zhou, J.; Esmaeili, P.; Zhang, X. Microbubble-enhanced recovery of residual bitumen from the tailings of oil sands extraction in a laboratory-Scalecale pipeline. *Energy Fuels* **2020**, *34*, 16476–16485.

(11) Kökpınar, M. A.; Göğüş, M. Critical flow velocity in slurry transporting horizontal pipelines. *J. Hydraul. Eng.* **2001**, *127*, 763–771.

(12) Kaushal, D.; Sato, K.; Toyota, T.; Funatsu, K.; Tomita, Y. Effect of particle size distri-

bution on pressure drop and concentration profile in pipeline flow of highly concentrated slurry. *Int. J. Multiphase Flow* **2005**, *31*, 809–823.

(13) Long, J.; Xu, Z.; Masliyah, J. On the role of temperature in oil sands processing. *Energy Fuels* **2005**, *19*, 1440–1446.

(14) Peker, S. M.; Helvaci, S. S. *Solid-liquid two phase flow*; Elsevier, 2011.

(15) Turian, R. M.; Yuan, T.-F. Flow of slurries in pipelines. *AIChE J.* **1977**, *23*, 232–243.

(16) Brown, N. P.; Heywood, N. I. *Slurry Handling: Design of solid-liquid systems*; Springer Science & Business Media, 1991.

(17) Doron, P.; Barnea, D. Flow pattern maps for solid-liquid flow in pipes. *Int. J. Multiphase Flow* **1996**, *22*, 273–283.

(18) Wilson, K. C.; Addie, G. R.; Sellgren, A.; Clift, R. *Slurry transport using centrifugal pumps*; Springer Science & Business Media, 2006.

(19) Su, L.; Xu, Z.; Masliyah, J. Role of oily bubbles in enhancing bitumen flotation. *Miner. Eng.* **2006**, *19*, 641–650.

(20) Wallwork, V.; Xu, Z.; Masliyah, J. Bitumen recovery with oily air bubbles. *Can. J. Chem. Eng.* **2003**, *81*, 993–997.

(21) Zhou, J. Z.; Li, H.; Chow, R. S.; Liu, Q.; Xu, Z.; Masliyah, J. Role of mineral flotation technology in improving bitumen extraction from mined Athabasca oil sands-II. Flotation hydrodynamics of water-based oil sand extraction. *Can. J. Chem. Eng.* **2020**, *98*, 330–352.

(22) Nguyen, A.; Schulze, H. Colloidal science of flotation marcel dekker. *New York* **2004**, 840.

(23) Zhang, X.; Kumar, A.; Scales, P. J. Effects of solvency and interfacial nanobubbles on surface forces and bubble attachment at solid surfaces. *Langmuir* **2011**, *27*, 2484–2491.

(24) Zhang, X.; Lohse, D. Perspectives on surface nanobubbles. *Biomicrofluidics* **2014**, *8*, 041301.

(25) Lohse, D.; Zhang, X., et al. Surface nanobubbles and nanodroplets. *Rev. Mod. Phys.* **2015**, *87*, 981.

(26) Zhou, Z.; Chow, R.; Cleyle, P.; Xu, Z.; Masliyah, J. Effect of dynamic bubble nucleation on bitumen flotation. *Can. Metall. Q.* **2010**, *49*, 363–372.

(27) Gu, G.; Sanders, R. S.; Nandakumar, K.; Xu, Z.; Masliyah, J. H. Hydrogen and oxygen bubble attachment to a bitumen drop. *Can. J. Chem. Eng.* **2004**, *82*, 846–849.

(28) Agarwal, A.; Ng, W. J.; Liu, Y. Principle and applications of microbubble and nanobubble technology for water treatment. *Chemosphere* **2011**, *84*, 1175–1180.

(29) Ashokkumar, M. The characterization of acoustic cavitation bubbles–an overview. *Ultrason. Sonochemistry* **2011**, *18*, 864–872.

(30) Li, M.; Bussonnière, A.; Bronson, M.; Xu, Z.; Liu, Q. Study of Venturi tube geometry on the hydrodynamic cavitation for the generation of microbubbles. *Miner. Eng.* **2019**, *132*, 268–274.

(31) Padilla-Martinez, J.; Berrospe-Rodriguez, C.; Aguilar, G.; Ramirez-San-Juan, J.; Ramos-Garcia, R. Optic cavitation with CW lasers: A review. *Phys. Fluids* **2014**, *26*, 122007.

(32) Huang, J.; Sun, L.; Liu, H.; Mo, Z.; Tang, J.; Xie, G.; Du, M. A review on bubble generation and transportation in Venturi-type bubble generators. *Exp. Comput. Multiph. Flow* **2020**, *2*, 123–134.

(33) Gao, Y.; Dashliborun, A. M.; Zhou, J. Z.; Zhang, X. Formation and stability of cavitation microbubbles in process water from the oilsands industry. *Ind. Eng. Chem. Res.* **2021**, *60*, 3198–3209.

(34) Baylar, A.; Ozkan, F.; Unsal, M. On the use of venturi tubes in aeration. *Clean J.* **2007**, *35*, 183–185.

(35) Carroll, J. J.; Slupsky, J. D.; Mather, A. E. The solubility of carbon dioxide in water at low pressure. *J. Phys. Chem. Ref. Data* **1991**, *20*, 1201–1209.

(36) Zhu, R.; Liu, Q.; Xu, Z.; Masliyah, J. H.; Khan, A. Role of dissolving carbon dioxide in densification of oil sands tailings. *Energy Fuels* **2011**, *25*, 2049–2057.

(37) Wallwork, V.; Xu, Z.; Masliyah, J. Processibility of Athabasca oil sand using a laboratory hydrotransport extraction system (LHES). *Can. J. Chem. Eng.* **2004**, *82*, 687–695.

(38) Schramm, L.; Stasiuk, E.; Yarranton, H.; Maini, B.; Shelfantook, B. Temperature effects from the conditioning and flotation of bitumen from oil sands in terms of oil recovery and physical properties. *J. Can. Pet. Technol.* **2003**, *42*.

(39) Cai, J.; Huai, X.; Li, X. Dynamic behaviors of cavitation bubble for the steady cavitating flow. *J. Therm. Sci.* **2009**, *18*, 338.

(40) Masliyah, J. H.; Czarnecki, J.; Xu, Z. Handbook on Theory and Practice on Bitumen Recovery from Athabasca Oil Sands. **2011**,

(41) Long, J.; Li, H.; Xu, Z.; Masliyah, J. H. Improving oil sands processability using a temperature-sensitive polymer. *Energy Fuels* **2011**, *25*, 701–707.

(42) Dhole, V. R.; Ramchandani, N.; Tainsh, R. A.; Wasilewski, M. Make your process water pay for itself. *Chem. Eng.* **1996**, *103*, 100.

(43) Zhou, Z.; Kasongo, T.; Xu, Z.; Masliyah, J. Assessment of bitumen recovery from the Athabasca oil sands using a laboratory denver flotation cell. *Can. J. Chem. Eng.* **2004**, *82*, 696–703.

(44) Xu, C.; Peng, S.; Qiao, G. G.; Gutowski, V.; Lohse, D.; Zhang, X. Nanobubble formation on a warmer substrate. *Soft Matter* **2014**, *10*, 7857–7864.

(45) Zhang, X. H.; Zhang, X. D.; Lou, S. T.; Zhang, Z. X.; Sun, J. L.; Hu, J. Degassing and temperature effects on the formation of nanobubbles at the mica/water interface. *Langmuir* **2004**, *20*, 3813–3815.

(46) Zhou, Z.; Xu, Z.; Finch, J.; Masliyah, J.; Chow, R. On the role of cavitation in particle collection in flotation–A critical review. II. *Miner. Eng.* **2009**, *22*, 419–433.

(47) Grau, R.; Heiskanen, K. Bubble size distribution in laboratory scale flotation cells. *Miner. Eng.* **2005**, *18*, 1164–1172.

(48) Abdulaziz, A. Performance and image analysis of a cavitating process in a small type venturi. *Exp. Therm. Fluid Sci.* **2014**, *53*, 40–48.

(49) Feng, Y.; Mu, H.; Liu, X.; Huang, Z.; Zhang, H.; Wang, J.; Yang, Y. Leveraging 3D printing for the design of high-performance venturi microbubble generators. *Ind. Eng. Chem. Res.* **2020**, *59*, 8447–8455.

(50) Yu, P.-W.; Ceccio, S. L.; Tryggvason, G. The collapse of a cavitation bubble in shear flows—A numerical study. *Phys. Fluids* **1995**, *7*, 2608–2616.

(51) Li, M.; Bussonnière, A.; Xiang, B.; Manica, R.; Liu, Q. Effect of solid wettability on three-phase hydrodynamic cavitation. *Miner. Eng.* **2022**, *180*, 107455.

(52) Kariznovi, M.; Nourozieh, H.; Abedi, J., et al. Measurement and correlation of viscosity and density for compressed Athabasca bitumen at temperatures up to 200^{o}C. *J. Can. Pet. Technol.* **2014**, *53*, 330–338.

(53) Isaacs, E.; Smolek, K. Interfacial tension behavior of Athabasca bitumen/aqueous surfactant systems. *Can. J. Chem. Eng.* **1983**, *61*, 233–240.

(54) Nourozieh, H.; Kariznovi, M.; Abedi, J., et al. Density and viscosity of Athabasca bitumen samples at temperatures up to 200C and pressures up to 10 MPa. *SPE Reserv. Evaluation Eng.* **2015**, *18*, 375–386.

(55) Schramm, L. L. The influence of suspension viscosity on bitumen rise velocity and potential recovery in the hot water flotation process for oil sands. *J. Can. Pet. Technol.* **1989**, *28*.

(56) Singh, M. K.; Ratha, D.; Kumar, S.; Kumar, D. Influence of particle-size distribution and temperature on rheological behavior of coal slurry. *Int. J. Coal Prep. Util.* **2016**, *36*, 44–54.

(57) Dai, Q.; Chung, K. H. Bitumen—sand interaction in oil sand processing. *Fuel* **1995**, *74*, 1858–1864.

(58) Liu, J.; Xu, Z.; Masliyah, J. Interaction between bitumen and fines in oil sands extraction system: Implication to bitumen recovery. *Can. J. Chem. Eng.* **2004**, *82*, 655–666.